bioRxiv preprint doi: https://doi.org/10.1101/2022.10.26.513911; this version posted October 26, 2022. The copyright holder for this preprint (which was not certified by peer review) is the author/funder, who has granted bioRxiv a license to display the preprint in perpetuity. It is made available under aCC-BY-NC-ND 4.0 International license.

Persistent lytic bacteriophage infection as a novel strategy for exploitation of nutrient-limited host bacteria

Authors

Jack Dorling[1,*], Naima Nhiri[2], Andrés Corral-Lugo[1,3], Eric Jacquet[2], Paulo Tavares[1,*]

Affiliation

[1] Université Paris-Saclay, CNRS, Institut de Biologie Intégrative de la Cellule (I2BC), UMR 9198, 91190, Gif-sur-Yvette, France

[2] Université Paris-Saclay, CNRS, Institut de Chimie des Substances Naturelles (ICSN), UPR 2301, 91198, Gif-sur-Yvette, France

[3] Present address: Intrahospital Infections Laboratory, National Centre for Microbiology, Instituto de Salud Carlos III (ISCIII), Madrid, Spain.

***Details of corresponding authors**

Jack Dorling and Paulo Tavares
Institut de Biologie Intégrative de la Cellule (I2BC)
Bâtiment 14B
1 Avenue de la Terrasse
91190 Gif-sur-Yvette,France
+33 (0) 1 69 82 38 60
jdg88673@tutanota.com
paulo.tavares@i2bc.paris-saclay.fr

Competing interests

The authors declare no competing financial interests

bioRxiv preprint doi: https://doi.org/10.1101/2022.10.26.513911; this version posted October 26, 2022. The copyright holder for this preprint (which was not certified by peer review) is the author/funder, who has granted bioRxiv a license to display the preprint in perpetuity. It is made available under aCC-BY-NC-ND 4.0 International license.

Abstract

Wild bacteria, from the open ocean to the gut, experience persistent nutrient limitation. This fundamentally affects bacterial physiology and metabolism and has profound impacts on their infection by bacterial viruses (bacteriophages). For virulent bacteriophages, which cannot enter a lysogenic state, this poses a problem for environmental persistence. Here we demonstrate that virulent bacteriophage SPP1 productively infects nutrient-limited stationary phase cultures of the Gram-positive bacterium *Bacillus subtilis*. Slow production and release of low numbers of infective viral particles resulted from a prolonged infection of the host population. Extensive culture lysis was greatly delayed, releasing additional viral particles and promoting fresh infections of bacterial survivors. Induced overproduction of cell surface bacteriophage receptor YueB, compensating for its scarcity in stationary phase, expedited infection dynamics under nutrient-limiting conditions, but did not change overall infection productivity. The temporal program of SPP1 gene expression differed from exponential phase, consistent with a prolonged, persistent mode of infection. Reduced expression of genes coding viral structural proteins correlated with the low yield of infectious particles. Importantly, exogenous influx of the carbon source maltose enhanced viral particle production. Our results uncover a novel adaptive strategy of a lytic phage for productive infection of nutrient-limited bacterial populations through persistent, exhaustive infection.

bioRxiv preprint doi: https://doi.org/10.1101/2022.10.26.513911; this version posted October 26, 2022. The copyright holder for this preprint (which was not certified by peer review) is the author/funder, who has granted bioRxiv a license to display the preprint in perpetuity. It is made available under aCC-BY-NC-ND 4.0 International license.

Introduction

In contrast to the highly-controlled, near ideal conditions under which most laboratory-based bacteriophage (phage)-bacteria infection studies are conducted, the growth and proliferation of wild bacteria is primarily restricted by limited or fluctuating carbon and energy supplies [1,2]. Availability of other nutrients [3,4] and physico-chemical environmental factors also limit bacterial growth [2,5]. These conditions are observed not only in aquatic and soil ecosystems but also in environments such as the mammalian gut where intense competition limits nutrient availability [6]. Consequently many environmental bacteria experience severe nutrient limitation and occupy a physiological state of slow or arrested metabolism known as 'starvation-survival' [1,7]. Growth rates in both aquatic and soil ecosystems are accordingly low [8–10] but bacterial densities may reach 10^5-10^6 colony forming units (CFU) ml^{-1} [5] or 10^9 CFU g^{-1} [11], in each respective environment, demonstrating the adaptation of bacteria to such oligotrophic conditions.

Phages depend upon their hosts' metabolism for multiplication [12,13]. However, global phage abundance is estimated to be higher than 10^{30} [14], even with considerable estimated environmental phage particle decay rates [15,16]. Thus, as bacteria have adapted to starvation-survival lifestyles, phages have conceivably adapted to exploit starving hosts. Such adaptive strategies remain largely unstudied in spite of their critical importance for phage persistence in natural ecosystems.

Phages exhibit varied infection strategies [13,15-19], ranging from lytic to lysogenic cycles. In lysogenic bacteria, chromosomally-integrated or episomal temperate phage genomes are maintained and propagated within the bacterial population [16]. Entry into lysogenic states and concomitant silencing of most phage gene expression is largely determined by host metabolic state upon infection [16,20]. However, strictly lytic (i.e. unable to establish a

bioRxiv preprint doi: https://doi.org/10.1101/2022.10.26.513911; this version posted October 26, 2022. The copyright holder for this preprint (which was not certified by peer review) is the author/funder, who has granted bioRxiv a license to display the preprint in perpetuity. It is made available under aCC-BY-NC-ND 4.0 International license.

lysogenic state) phages persist in soil and aquatic environments. This raises the fundamental questions of if and how lytic phages are able to overcome the challenges of infecting starving hosts. Indeed, it is often implicitly assumed that such phages require exponentially growing bacteria in order to stage productive infections.

To address this dearth of information, we investigated whether a strictly lytic phage could productively exploit a non-growing, nutrient limited host. To do so, we employed the model Gram-positive soil bacterium *Bacillus subtilis*, which displays numerous adaptations to nutrient limiting conditions [21,22] and its lytic siphovirus Subtilis Phage Pavia 1 (SPP1) [23]. SPP1 infection of *B. subtilis* starts with reversible adsorption to cell wall teichoic acids, irreversible adsorption to the protein YueB [24], and transfer of naked phage DNA into the bacterial cytoplasm [25,26]. These processes depend on the presence of Ca^{2+} and host membrane potential [27,28]. Under optimised laboratory conditions phage DNA is delivered to the cell within the first 3min [28], followed by early gene expression and genome replication [29,30]. Late gene expression begins after 10-12min and virion assembly ensues [31]. After ~30-60min host cells lyse, liberating ~200 viral particles per cell [32]. Previous work suggested that SPP1 may only be able to infect growing bacteria [33].

Here we report the discovery of a low productivity stationary phase (SP) infection strategy of *B. subtilis* by SPP1. The greatly prolonged infection of most of the bacterial population, the low yield of infectious particles (or virions) and gene expression patterns differ significantly from infection of exponentially growing bacteria. Such a persistent infection mode of nutrient-limited *B. subtilis* bacteria represents a resiliency strategy to promote sustainability of lytic phage populations under conditions that do not sustain host bacterial growth.

bioRxiv preprint doi: https://doi.org/10.1101/2022.10.26.513911; this version posted October 26, 2022. The copyright holder for this preprint (which was not certified by peer review) is the author/funder, who has granted bioRxiv a license to display the preprint in perpetuity. It is made available under aCC-BY-NC-ND 4.0 International license.

Materials and Methods

Bacteria and phage strains

Bacterial and phage strains are in **Table S1**. *B. subtilis* 168 strain 1A1 [34] (*Bs*^{wt}) was the wild-type strain. Strain YB886 [35] was used for phage amplification and titration. *B. subtilis* strain *Bs*$^{Pspac::yueB}$ over-expresses the SPP1 receptor YueB in the presence of IPTG. Either wild-type SPP1 (SPP1^{wt}) or SPP1 expressing an mNeonGreen reporter (SPP1^{mNeonGreen}) were used for infection experiments.

Bs$^{Pspac::yueB}$ and SPP1^{mNeonGreen} were constructed as described in **Supplementary Material and Methods**. Primers used are in **Table S2**.

Bacteria growth and phage infection

Bacteria were cultured in LB medium at 37^{o}C unless otherwise stated. Experiments were either performed in flasks or in 96-well plates in a Tecan plate reader. Bacterial CFU were enumerated by serial dilution and plating. CFU originating from spores were enumerated by the same method after heating the sample to 80^{o}C for 20 minutes. Phage infections were made using 2×10^{9}PFU ml^{-1} with the addition of 10mM $CaCl_2$. Phages were enumerated by serial dilution and titration in semi-solid agar. For free phage populations only sample supernatant was titrated [33]. For total phage populations the entire sample was mixed with chloroform, left on ice for >2h and titrated. SPP1 irreversible adsorption (IA) was measured as described in [24].

Microscopy

bioRxiv preprint doi: https://doi.org/10.1101/2022.10.26.513911; this version posted October 26, 2022. The copyright holder for this preprint (which was not certified by peer review) is the author/funder, who has granted bioRxiv a license to display the preprint in perpetuity. It is made available under aCC-BY-NC-ND 4.0 International license.

For microscopy, bacteria were placed on a water-agarose pad and imaged using an Axio Observer Z1 microscope with a 63x oil immersion lens (Zeiss; Marly Le Roi, France). DAPI and GFP filter sets were used to image TMA-DPH and mNeonGreen/AlexaFluor 488 fluorophores, respectively. Post-capture image processing was carried out using Fiji [36]. MicrobeJ [37] was used to extract morphological and fluorescence data from microscopy images. After background fluorescence correction infected cells were identified as those exhibiting mNeonGreen fluorescence intensity greater than +4·SD above the mean fluorescence of non-infected cells. This was verified by manual counting (**Supplementary figure 1**).

RNA and protein methods

For RNA and protein isolation, samples were mixed with sample stop buffer containing 100mM NaN_3, supernatant thoroughly removed, pellets frozen in liquid nitrogen and stored at -80ºC. RNA was extracted with a 'NucleoSpin RNA Mini' RNA purification kit (Macherey-Nagel). Samples were purified twice with an extra DNase digestion step between purifications. RNA was quantified using a Nanodrop One spectrophotometer (ThermoFisher Scientific) and RNA integrity verified using an Agilent 2100 bioanalyzer (Agilent Technologies). 200ng total RNA was then used to produce cDNA. Quantitative real-time PCR (qRT-PCR) was performed on a QuantStudio 12K Flex Real-Time PCR System (Life Technologies) with a SYBR green detection protocol. Data normalisation was performed with five *B. subtilis* reference genes. Relative gene expression ratios were determined using the ΔΔCt method with a Ct limit of 33 cycles.

bioRxiv preprint doi: https://doi.org/10.1101/2022.10.26.513911; this version posted October 26, 2022. The copyright holder for this preprint (which was not certified by peer review) is the author/funder, who has granted bioRxiv a license to display the preprint in perpetuity. It is made available under aCC-BY-NC-ND 4.0 International license.

Protein was extracted as described previously [38]. Approximate protein concentrations were verified by intensity of Coomassie staining of gels and Western-blot detection of gp11 was carried out with a rabbit polyclonal α-gp11 antibody [39].

Quantitative and statistical data analyses

Analyses were performed using R version 3.6.3 [40]. Growth and lysis rates were derived using the smooth.spline and predict packages [40]. All statistical analyses involving more than 2 independent groups were performed using linear modelling. The package lm was used to fit general linear models (LM's) to normally distributed, constant variance (or transformed) data, and glm to fit generalised linear models (GLM's) to untransformed data requiring different error structures or link functions. Piece-wise regression analyses breakpoints were performed using the segmented R package [41]. Multiple comparisons were made using either multcomp [42] or emmeans [43] packages. Model predictions for visual representation were generated using the predict package. Two-tailed t-tests or Wilcoxon rank sum tests were performed using appropriate R packages [40]. Pearsons correlation coefficients were calculated using the cor package [40].

Further details of Materials and Methods are provided in **Supplementary Material and Methods**.

Results

Assessment of onset nutrient limitation during the *B subtilis* growth cycle

Growth and morphological characteristics of Bs^{wt} were studied during its growth cycle in LB medium to determine the timing of growth arrest and nutrient limitation. Cell size was used

bioRxiv preprint doi: https://doi.org/10.1101/2022.10.26.513911; this version posted October 26, 2022. The copyright holder for this preprint (which was not certified by peer review) is the author/funder, who has granted bioRxiv a license to display the preprint in perpetuity. It is made available under aCC-BY-NC-ND 4.0 International license.

as a proxy for nutrient limitation [44–46]. Detectable growth halted from ~5h onward (**Supplementary figure 2a**, **inset**), clearly delimiting periods of growth and non-growth. Transition phase (TP) was designated as the period between 4-6h, preceded by exponential phase (EP) and followed by SP. This determined time-points to study phage infection during different host growth phases. We observed a decline in SP OD_{600} between ~9 and 30h (**Supplementary Fig. 2a**), though viable cell counts indicated no significant cell death throughout this period (**Supplementary Fig. 2b**). This was accompanied by a reduction of cell length with culture age (**Supplementary figure 2c**) while cell width varied little resulting in a concomitant reduction of surface area and volume. By 10h post-inoculation ≥97.1% of cells had reached 'minimal' cell dimensions as demonstrated by their similarity to those at 30h (**Supplementary figure 2d; Supplementary Data Analysis**). Cell length reduction thus explained the reduction of culture OD_{600} during SP without loss of cell viability. As bacteria adopt a smaller size under nutrient poor conditions [44,45], we concluded that nutrient limitation increased with time, and that by 10h post-inoculation cells could be considered non-growing and nutrient-limited.

SPP1 infection during different *B. subtilis* growth cycle stages

The zone of clearance within SPP1 phage plaques does not grow detectably after reaching a defined size, though lysis halo formation is observed (**Supplementary figure 3**). We hypothesised that this results from an inability of SPP1 to infect bacteria in SP. We thus decided to examine the efficiency of SPP1 infection at selected time-points during the *B subtilis* growth cycle in liquid medium (**Fig. 1a**). Infection efficiency, assessed by culture lysis (**Fig. 1b**) and free PFU production (**Fig. 1c**), gradually decreased with bacterial growth rate phase**.** Indeed, EP and early transition phase (eTP) infected cultures lost OD_{600} more rapidly

bioRxiv preprint doi: https://doi.org/10.1101/2022.10.26.513911; this version posted October 26, 2022. The copyright holder for this preprint (which was not certified by peer review) is the author/funder, who has granted bioRxiv a license to display the preprint in perpetuity. It is made available under aCC-BY-NC-ND 4.0 International license.

over time than non-infected cultures, while late transition phase (lTP) or SP infected cultures did not (**Fig. 1b; Table S3)**. Only EP and eTP infections resulted in net PFU production (**Fig. 1c**). These initial experiments were limited to a 2h window post-infection (p.i.). After 2h of infection in SP, little lysis had occurred but the number of free infectious phages had clearly decreased below the input level (**Fig. 1c**). This led us to the hypothesis that phage adsorption and inactivation had occurred and that infection may occur but more slowly than under nutrient-replete conditions. Therefore, we infected SP cells as previously and followed infection for 18h. During this longer p.i. period slow lysis of the infected culture occurred (**Fig. 1d**) and by 18h p.i. a ~5-fold net increase in free infectious phage particles relative to the input level was observed (**Fig. 1e**).

Dynamics of SPP1 infection of *B subtilis* during stationary-phase

We then continuously monitored, over a 30h period, the infection of Bs^{wt} by $SPP1^{wt}$ during different growth phases using a plate-reader-based setup. Lysis was evident in all infected cultures (orange triangles in **Fig. 2a**) relative to non-infected controls (grey circles in **Fig. 2a**). Infection duration increased with culture age (**Fig. 2b**). Cultures infected early during TP displayed multiphasic lysis behavior while late in TP and SP a single phase of slow lysis preceded a single more rapid lysis phase (**Fig. 2a**).

We then used a flask-based setup to simultaneously monitor OD_{600}, viable cell counts, phage yield and infection prevalence at the single-cell level, using the reporter phage $SPP1^{mNeonGreen}$. As expected, slow, but statistically significant lysis was evident in the first 10h of infection (**Fig. 3a**; analysis of covariance; $F_{1,12}^{time:infection\_status} = 71.9$, $p < 0.001$) and was accompanied by a significant reduction in CFU recovered from infected cultures following phage-induced lysis (green triangles in **Fig. 3b**). In contrast, no differences were

bioRxiv preprint doi: https://doi.org/10.1101/2022.10.26.513911; this version posted October 26, 2022. The copyright holder for this preprint (which was not certified by peer review) is the author/funder, who has granted bioRxiv a license to display the preprint in perpetuity. It is made available under aCC-BY-NC-ND 4.0 International license.

found between infected and non-infected cultures in the proportion of CFU originating from spores (diamonds and squares in **Fig. 3b**, respectively; ordinate on the right), which are resistant to SPP1 infection. Sporulation frequency increased over time in all cultures reaching ~2.5-2.8% by 40h post-inoculation. This indicated that SPP1 infection of the bacterial population did not appreciably affect the developmental decision of *B. subtilis* to sporulate under nutrient limitation [47]. Immediately after infection, free phage numbers dropped 3.4 ± 0.3-fold relative to the input due to their engagement in infection. After a period of ~2h, phage counts increased at a relatively steady rate from 2 to 10h p.i. in both free and total phage populations (**Fig. 3c**, **Table S3**). This coincided with steady culture lysis in the first 10h p.i. (**Fig. 3a**). Between 10h and 30h p.i. further phage multiplication had occurred with a convergence in the number of phages found in free and total populations during this period (**Fig. 3c**, Wilcoxon rank sum test$^{30h\ p.i.}$; W = 6, p = 0.686). This indicated release of most intracellular PFU into the extracellular environment and coincided with extensive culture lysis.

In parallel, we imaged infected cultures to examine infection propagation within the bacterial population. To do so we used a phage engineered to express the fluorescent reporter mNeonGreen under the control of the SPP1 *P*E2 early promoter. Control experiments conducted in EP, where infection prevalence is known to be ~100%, showed that SPP1^{mNeonGreen} robustly reported infection in only ~72% of the bacterial population at 1h p.i. (**Supplementary Fig. S4**). This is due to the time required for mNeonGreen folding and fluorophore maturation, leading to some underestimation of the number of infected cells at defined time points. This caveat in mind, we documented a very slow initial increase in the proportion of visibly infected, mNeonGreen-bright, cells in SP (**Fig. 3d,e**) before a more rapid increase until observations were halted at 10h p.i. (**Fig. 3d,e**). Interestingly, despite the major

bioRxiv preprint doi: https://doi.org/10.1101/2022.10.26.513911; this version posted October 26, 2022. The copyright holder for this preprint (which was not certified by peer review) is the author/funder, who has granted bioRxiv a license to display the preprint in perpetuity. It is made available under aCC-BY-NC-ND 4.0 International license.

237 release of intracellular phage particles between 10-30h and the lysis of 98.5 ± 2.4% cells in
238 the culture, 46.7 ± 2.3% of the remaining cells were visibly infected at 30h p.i. (**Fig. 3e**).
239
240 **Irreversible adsorption's (IA) role in determining stationary-phase infection dynamics**
241 The essential step determining phage infection initiation is irreversible adsorption (IA) to the
242 host cell. SPP1 irreversible binding to the bacterial receptor YueB [48] and the resulting
243 inactivation of input phages is considered a proxy for the number of phages that engage in
244 host infection [49]. The 3.4 ± 0.3-fold reduction in the titre of free infectious phages observed
245 upon mixing of SPP1 with SP cells showed that SPP1 adsorbs relatively rapidly to nutrient
246 deprived bacteria (**Fig. 3c**).
247 Availability of YueB at the bacterial surface is critical for SPP1 IA [48]. In order to investigate
248 if this could be a limiting factor for SPP1 infection during SP we used immunofluorescence
249 microscopy to quantify the proportion of cells exposing detectable amounts of receptor and,
250 where present, cell surface YueB abundance at different stages of the *B. subtilis* growth
251 cycle (**Supplementary figure 5a,b**). This was performed using Bs^{wt} and an isogenic strain
252 overproducing YueB under the control of an IPTG-inducible promoter ($Bs^{Pspac::yueB}$)
253 (**Supplementary figure 5b, c**). The number of cell surface YueB foci decreased through TP
254 (4-6h) into SP (10h) in both strains, though significantly more rapidly in Bs^{wt}
255 (**Supplementary figure 5c**, analysis of covariance; $\chi^{2\ \text{time\_point:strain}} = 804$, df = 3, $p < 0.001$).
256 In parallel, the proportion of cells without detectable YueB foci increased sharply to 30.2%
257 as Bs^{wt} entered into eTP, remaining high in ITP (53%) and SP (46.5%) (**Supplementary**
258 **figure 5c**). This limitation was overcome in $Bs^{Pspac::yueB}$ where surface exposed receptor was
259 present on all cells (**Supplementary figure 5c**).

bioRxiv preprint doi: https://doi.org/10.1101/2022.10.26.513911; this version posted October 26, 2022. The copyright holder for this preprint (which was not certified by peer review) is the author/funder, who has granted bioRxiv a license to display the preprint in perpetuity. It is made available under aCC-BY-NC-ND 4.0 International license.

We then measured IA efficiency of SPP1^{wt} to both strains throughout the growth cycle. The two strains showed identical growth properties (**Supplementary figure 5a**) but drastically different profiles of phage SPP1 IA over the course of the growth cycle (**Fig. 4a**). During EP *Bs*^{wt} and *Bs*$^{Pspac::yueB}$ had an IA of 99.2 ± 0.5 and 99.9 ± 0.007% of all added phages at 10min post-phage addition, respectively (**Fig. 4a**). From 4h post-inoculation onward (eTP through SP growth phases), *Bs*^{wt} bacteria supported IA of only ~85-88% of all added phages while *Bs*$^{Pspac::yueB}$ retained a ~99.9% IA throughout its growth cycle (**Fig. 4a**).

Significantly higher IA to *Bs*$^{Pspac::yueB}$ than to *Bs*^{wt} prompted study of IA's impact on the dynamics of SPP1 infection in SP. *Bs*$^{Pspac::yueB}$ lysed more rapidly than *Bs*^{wt} during SP infection, albeit exhibiting some variability among experiments (**Fig. 4b,c**) that was reflected in the numbers of free PFU observed (**Fig. 4d**). In spite of this variability, the *Bs*$^{Pspac::yueB}$ total phage yield was remarkably reproducible (**Fig. 4e**). The rate of phage production in Bs$^{Pspac::yueB}$ cultures was faster than during infection of *Bs*^{wt} but, interestingly, the final phage yield at 30h p.i. was very similar (**Fig. 4d, e**).

SPP1 gene expression during stationary phase infection of *B. subtilis*

The radically different dynamics and low yield of SP SPP1 infection prompted us to compare phage gene expression during SP infection with that of highly efficient EP infection. Using qRT-PCR we quantified mRNA expression of early genes *35* (recT-like recombinase [50]) and *46* (putative host take-over gene), of the late genes *6* and *11* (SPP1 procapsid assembly proteins), and of the late lysis genes *24.1* and *26* (**Fig. 5a**) [51,52]. qRT-PCR data were calibrated firstly to uninfected early EP samples to clearly assess patterns of early and late gene expression, and secondly to 8min p.i. EP samples for comparative gene expression analysis across different EP and SP infection time-points (**Fig. 5b**).

bioRxiv preprint doi: https://doi.org/10.1101/2022.10.26.513911; this version posted October 26, 2022. The copyright holder for this preprint (which was not certified by peer review) is the author/funder, who has granted bioRxiv a license to display the preprint in perpetuity. It is made available under aCC-BY-NC-ND 4.0 International license.

During EP infection (**Supplementary figure 6a-c**) early gene expression was clearly dominant at 8min p.i. while stronger expression of late genes was evident at 25min p.i. (**Fig. 5b**, *left panels*). Between these two time points the early gene *46* was downregulated while early gene *35* was approximately equivalently transcribed (**Fig. 5b**).

During infection of SP cultures (**Supplementary figure 6d-f**) the transcriptional profile of SPP1 was very different (**Fig. 5b,** *right panels*). Phage gene expression increased more slowly than during EP infections as highlighted by calibration to infected early EP samples (**Fig. 5b**, *bottom*). The SPP1 expression temporal program in SP was far more homogeneous, displaying reduced late gene expression relative to early gene expression (**Fig. 5b**, *top*). At 1h p.i., expression of early genes was slightly higher than late genes while at 6 and 10h no differences in expression of the examined genes were observed (**Fig. 5b**, *top right*). Expression of early genes *35* and *46* in infected SP cells took 6 and 10 h, respectively, to reach approximately the same expression observed at 8 min p.i. of EP cells **(Fig. 5b**, *bottom*). Moreover, expression of late genes encoding SPP1 structural and lysis proteins at these time points p.i. was significantly lower than at 25min p.i. during EP **(Fig. 5b**, *top* and *bottom*; **Table S4**). Interestingly, the ~24.5- and ~11-fold lower expression of genes essential for viral particle assembly at 6 and 10 h p.i. in SP bacteria (**Table S4**), respectively, correlates particularly well with the reduction in yield of viable SPP1 particles relative to EP infection (**Supplementary figure 6c,f**). These numbers provide a good proxy of differences between infected cells at EP and SP as a large majority of cells are infected in both populations at the time points compared, as denoted by their lysis behavior (**Supplementary figure 6a,d,e**).

Intriguingly, the pattern of SP gene expression at 30h p.i. resembles that of early EP, though exhibiting higher expression of gene *35*. This occurs following extensive lysis of the infected

bioRxiv preprint doi: https://doi.org/10.1101/2022.10.26.513911; this version posted October 26, 2022. The copyright holder for this preprint (which was not certified by peer review) is the author/funder, who has granted bioRxiv a license to display the preprint in perpetuity. It is made available under aCC-BY-NC-ND 4.0 International license.

culture (**Supplementary figure 6d-e**). Many (40.9 ± 14%) of the surviving cells at this time were detectably infected as revealed by fluorescence imaging of the SPP1^{mNeonGreen} reporter gene (**Supplementary figure 6g**). This may indicate new infections of a small fraction of previously uninfected cells.

Reduced transcription of late genes required for assembly of viral particles is a distinctive feature of SP infected cells and provides an explanation for the low yield of PFU. We thus monitored the production of gp11, a scaffolding protein present in hundreds of copies per SPP1 procapsid [53]. Strong expression of its encoding gene *11* in late EP (**Fig. 5b**, *left*) correlated with strong production of gp11 after 25min of EP infection (**Fig. 5c**). In contrast, after 1h of SP infection gp11 was present in very low quantities, and significantly less than at 8min EP p.i., demonstrating the slow pace of SP infection at the molecular level. SP gp11 levels initially increased, remaining roughly constant after 6h p.i., though in clearly lower quantities than during EP (**Fig. 5c**).

The impact of nutrient influx on the outcome of stationary phase infection

Our results show that the duration and productivity of the infectious cycle of SPP1 are radically altered upon infection of nutrient-limited bacteria, notwithstanding the large number of bacteria infected. We posited that this persistent infection state of the host population would enable SPP1 to multiply rapidly when new nutrients become available, stimulating bacterial metabolism. To test this hypothesis we grew *Bs*^{wt} in a plate reader and infected cells at SP before supplementation with maltose (15mM) at 0, 1, 4 and 8h p.i. (**Fig. 6a**). Maltose is an energy-rich carbon source that causes only very weak carbon catabolite repression in *B. subtilis* [54].

bioRxiv preprint doi: https://doi.org/10.1101/2022.10.26.513911; this version posted October 26, 2022. The copyright holder for this preprint (which was not certified by peer review) is the author/funder, who has granted bioRxiv a license to display the preprint in perpetuity. It is made available under aCC-BY-NC-ND 4.0 International license.

Maltose addition abrogated the reduction of OD_{600} observed during late SP (dark grey curves in **Fig. 6b**). Supplementation with maltose of infected bacteria in SP led to extensive, synchronised, lysis of infected cultures reaching 50% of the maximal OD_{600} at ~10.5h p.i, irrespective of the time of its addition (**Fig. 6b**). Lysis occurred later and less abruptly in absence of exogenous maltose (50 % of the maximal OD_{600} after ~12h p.i.).

Approximately 6.5 h after lysis, cultures supplemented with maltose resumed exponential growth, likely nourished by maltose and the pool of nutrients released from previously lysed cells (**Fig. 6b**). These cells were infected by SPP1 as demonstrated by the significantly higher number of total phages relative to free phages in the culture at the end of the experiment (**Fig. 6c**). This effect was amplified in experiments performed in flasks (**Fig. 6d**). In contrast, infected cultures that were not supplemented with maltose lysed later, regrew only very poorly within the experimental time-frame (**Fig. 6b**), and most phage particles were free in the culture at the end of the experiment (**Fig. 6c**).

Discussion

We report the discovery that lytic bacteriophage SPP1 stages persistent, productive infections in planktonic cultures of nutrient-limited *B subtilis*. In this persistent infection mode, the infection cycle spans >10h. Lysis initiates slowly, followed by a rapid mass lysis phase. It is unlikely that lysis of bacteria from without [55] occurs because SPP1 particles do not kill *B. subtilis* upon contact and non-infected cells are insensitive to the SPP1 lysin gp25 released from lysed bacteria in liquid culture [56]. A vast majority of cells in SP are therefore infected, with lysis resulting from complete infection cycles. The pace and overall productivity of this persistent SP infection mode contrasts starkly with that of rapid, highly productive EP infections (**Figs. 1,2**). We conclude that SPP1 is equipped for fast and

bioRxiv preprint doi: https://doi.org/10.1101/2022.10.26.513911; this version posted October 26, 2022. The copyright holder for this preprint (which was not certified by peer review) is the author/funder, who has granted bioRxiv a license to display the preprint in perpetuity. It is made available under aCC-BY-NC-ND 4.0 International license.

efficient multiplication in metabolically active host cells, but also for engaging a persistent infection mode for its environmental maintenance under adverse conditions. This adaptive strategy offers an explanation for how lytic phages may maintain their abundance in natural ecosystems such as the soil where bacteria, like *B subtilis*, exist primarily in nutrient-limited stationary phase [1,2]. Under such conditions, a pool of virions would be renewed by persistent infection while infrequent blooms of exponentially growing host bacteria would be efficiently exploited for major phage amplification.

Discovery of this persistent infection mode prompted investigation of how landmark steps of the viral infectious cycle were affected. Phage adsorption to host cells, the first step of infection, is impacted by scarcity of the SPP1 receptor YueB at the bacterial cell surface [24,25]. The effect of reduced SP cell surface YueB abundance was assessed experimentally in a strain overproducing YueB that maintains very high levels of SPP1 irreversible adsorption through the complete bacterial growth cycle (**Fig 4a**). More rapid extensive lysis of this strain (**Fig. 4b,c**) showed that limited YueB availability in wild-type SP *B. subtilis* extends the overall infection period in the bacterial population. Overall scarcity and cell-to-cell variation of YueB abundance (**Supplementary figure 5b,c**) possibly leads to some asynchrony of infection initiation. However, infected wild type bacteria still undergo a rather rapid extensive lysis phase (**Fig. 4b,c**) indicating that the long infection cycle duration minimizes this asynchrony effect. SPP1 multiplied faster in the YueB-overproducing strain but, strikingly, the final yield of infectious particles was identical to the wild type strain (**Fig. 4d,e**). Collectively, these results show that SPP1 adsorption to SP *B subtilis* impacts infection dynamics but does not determine the overall yield of virions produced during infection of a given SP bacterial population. Phage yield is therefore mostly determined by the limited metabolic capacity of nutrient-limited cells.

bioRxiv preprint doi: https://doi.org/10.1101/2022.10.26.513911; this version posted October 26, 2022. The copyright holder for this preprint (which was not certified by peer review) is the author/funder, who has granted bioRxiv a license to display the preprint in perpetuity. It is made available under aCC-BY-NC-ND 4.0 International license.

379 The program of SPP1 gene expression differs significantly between EP and SP infection
380 both in temporal program and overall gene expression (**Fig. 5b**). Unlike EP infection, during
381 persistent SP infection the expression of early and late genes remained roughly similar until
382 extensive lysis. Importantly, late in infection, an ~11-fold reduction of transcription of genes
383 encoding proteins essential for virions assembly was observed relative to late EP infection
384 (**Fig. 5b**; **Table S4**). This reduction correlates particularly well with the decrease in number
385 of virions produced during persistent SP infection relative to rapid EP infection
386 (**Supplementary figure 6c,f**). Reduction of expression of genes encoding phage structural
387 proteins is particularly meaningful in the context of a nutrient-deprived host cell because
388 production of virion components represents the highest biosynthetic and energetic cost
389 during infection [38,57]. Therefore, SPP1 pervasively infects SP bacterial populations for a
390 long period, effecting multiplication at reduced costs to the cell to achieve successful
391 infection under adverse conditions.
392 Expression of SPP1 lysis genes *24.1* and *26* [58] is also lower than during late EP infection
393 (**Fig. 5b**; **Table S4**). Such reduction does not hinder the capacity of SPP1 to promote SP
394 cell lysis, and efficient release of virions into the environment is ensured. When a
395 carbon/energy source (maltose) is made available to the infected SP culture lysis is more
396 rapid. However, the time of maltose addition did not affect lysis behaviour (**Fig. 6b**). We
397 conclude that the molecular clock for phage-induced host cell lysis is set upon infection
398 initiation and that the added exogenous carbon source only renders lysis more effective.
399 The exact mechanism by which this occurs is currently unknown. Interestingly, infected
400 cultures supplemented with maltose re-grow after extensive phage-induced lysis and are
401 clearly re-infected (**Fig. 6b-d**). Such re-growth, fueled by maltose and likely by nutrients
402 released from lysed bacteria, offers SPP1 the opportunity for a new infection cycle mimicking

bioRxiv preprint doi: https://doi.org/10.1101/2022.10.26.513911; this version posted October 26, 2022. The copyright holder for this preprint (which was not certified by peer review) is the author/funder, who has granted bioRxiv a license to display the preprint in perpetuity. It is made available under aCC-BY-NC-ND 4.0 International license.

403 conditions of host encounter of new nutrients. Indeed, un-supplemented cultures do not re-
404 grow significantly but the low population of cells surviving mass culture lysis are extensively
405 infected (**Fig. 3d,e**) and feature a pattern of SPP1 gene expression reminiscent of early EP
406 infection (**Fig. 5b**).
407 Infection in stationary phase was previously reported for several phages [17,59–63] but their
408 modes and dynamics of infection remain largely uncharacterised [62]. Phage T7 has the
409 remarkable capacity for productive infection of stationary phase bacteria [59]. Other lytic
410 phages adopt a dormant state in such nutrient-limited bacteria. In pseudo-lysogeny lytic
411 phage DNA resides in the cell in an inactive state [18,63] while in the hibernation mode,
412 described for phage T4, some early genes are expressed but the infection cycle is halted
413 until further nutrients become available to the host cell [17]. In contrast, the above presented
414 SPP1 persistent infection mode involves a complete productive infection process. Here, we
415 investigated this infection mode in a simplified single phage-host pair laboratory based setup
416 in order to carry out a detailed characterisation of their interaction. The soil environment
417 imposes much more complex, multi-factorial, constraints to the SPP1-*B subtilis* interaction
418 [62,64]. Nevertheless, SPP1's persistent infection mode appears to represent an adaptive
419 strategy that would aid persistence of lytic phage populations under frequently encountered
420 environmental conditions that heavily restrict host bacterial growth. Infected nutrient-limited
421 cells are killed and phage particles released. Environmental decay of free phage particles is
422 a threat for these free particles [65]. However, nutrients liberated by lysis can also fuel new
423 infections of surviving susceptible host cells. This will sustain local phage populations in the
424 medium term while awaiting nutrient influx, while additional phage particles may be
425 disseminated to find new susceptible hosts.
426

bioRxiv preprint doi: https://doi.org/10.1101/2022.10.26.513911; this version posted October 26, 2022. The copyright holder for this preprint (which was not certified by peer review) is the author/funder, who has granted bioRxiv a license to display the preprint in perpetuity. It is made available under aCC-BY-NC-ND 4.0 International license.

Author contributions

JD and PT designed the research. JD performed most experimental work with help from PT. NN and EJ performed qRT-PCR, including preceding validation and quality assessment work. ACL designed and constructed SPP1^{mNeonGreen}. Data were analysed by NN, EJ and JD. Data were interpreted by JD and PT. The manuscript was written by JD, EJ and PT. Work was read and critically revised by JD and PT. All authors approved the final version of the manuscript.

Acknowledgments

We thank Sriram Tiruvadi-Krishnan for providing the plasmid bearing the *mNeonGreen* gene codon-optimised for *B. subtilis*. This work was funded by Fondation pour la Recherche Médicale (Equipe FRM), grants ANR BacVirRemodel and ANR BioBrickEvolver, and institutional funding from CNRS.

Competing interests

The authors declare no competing financial interests.

bioRxiv preprint doi: https://doi.org/10.1101/2022.10.26.513911; this version posted October 26, 2022. The copyright holder for this preprint (which was not certified by peer review) is the author/funder, who has granted bioRxiv a license to display the preprint in perpetuity. It is made available under aCC-BY-NC-ND 4.0 International license.

References

[1] Morita RY. The starvation-survival state of microorganisms in nature and its relationship to the bioavailable energy. *Experientia* 1990; **46**: 813–7.

[2] Hobbie JE, Hobbie EA. Microbes in nature are limited by carbon and energy: The starving-survival lifestyle in soil and consequences for estimating microbial rates. *Front Microbiol* 2013; **4**: 1–11.

[3] Tyrrell T. The relative influences of nitrogen and phosphorus on oceanic primary production. *Nature* 1999; **400**: 525–31.

[4] Arrigo KR. Marine microorganisms and global nutrient cycles. *Nature* 2005; **437**: 343–8.

[5] Egli T. How to live at very low substrate concentration. *Water Res* 2010; **44**: 4826–37.

[6] Reese AT, Pereira FC, Schintlmeister A, Berry D, Wagner M, Hale LP, et al. Microbial nitrogen limitation in the mammalian large intestine. *Nat Microbiol* 2018; **3**: 1441–50.

[7] Kolter R. The Stationary Phase of the Bacterial Life Cycle. *Annu Rev Microbiol* 1993; **47**: 855–74.

[8] Day JW, Hall CAS, Kemp WM, Yanez-Arancibia A. *Estuarine ecology*. Wiley-Blackwell; 2013.

[9] Pomeroy LR, le Williams PJB, Azam F, Hobbie JE. The microbial loop. *Oceanography* 2007; **20**: 28–33.

[10] Coleman DC, Mac A. Callaham J, Crossley DA. *Fundamentals of Soil Ecology.* 3th Ed. Academic Press, 2018.

[11] Whitman WB, Coleman DC, Wiebe WJ. Prokaryotes: The unseen majority. *Proc Natl Acad Sci* 1998; **95**: 6578–83.

[12] Kokjohn TA, Sayler GS, Miller R V. Attachment and replication of *Pseudomonas aeruginosa* bacteriophages under conditions simulating aquatic environments. *J Gen Microbiol* 1991; **137**: 1–6.

[13] Zimmerman AE, Howard-Varona C, Needham DM, John SG, Worden AZ, Sullivan MB, *et al.* Metabolic and biogeochemical consequences of viral infection in aquatic ecosystems. *Nat Rev Microbiol* 2019; **18:** 21–34.

[14] Hendrix RW. Bacteriophages: Evolution of the Majority. *Theor Popul Biol* 2002; **61**: 471–80.

[15] Clokie MRJ, Millard AD, Letarov A V., Heaphy S. Phages in nature. *Bacteriophage* 2011; **1**: 31–45.

bioRxiv preprint doi: https://doi.org/10.1101/2022.10.26.513911; this version posted October 26, 2022. The copyright holder for this preprint (which was not certified by peer review) is the author/funder, who has granted bioRxiv a license to display the preprint in perpetuity. It is made available under aCC-BY-NC-ND 4.0 International license.

[16] Abedon SA. *Bacteriophage Ecology*. Cambridge University Press; 2008.

[17] Bryan D, El-shibiny A, Hobbs Z, Porter J, Kutter EM. Bacteriophage T4 Infection of Stationary Phase *E. coli*: Life after Log from a Phage Perspective. *Front Microbiol* 2016; **7**: 1–12.

[18] Romig WG, Brodetsky AM. Isolation and preliminary characterization of bacteriophages for *Bacillus subtilis*. *J Bacteriol* 1961; **82**: 135–41.

[19] Wilson WH, Carr NG, Mann NH. The effect of phosphate status on the kinetics of cyanophage infection in the oceanic cyanobacterium *Synechococcus* sp. WH7803. *J Phycol* 1996; **32**: 506–16.

[20] Laganenka L, Sander T, Lagonenko A, Chen Y, Link H, Sourjik V. Quorum Sensing and Metabolic State of the Host Control Lysogeny-Lysis Switch of Bacteriophage T1. *MBio* 2019; **10**: 3–8.

[21] Lopez D, Vlamakis H, Kolter R. Generation of multiple cell types in *Bacillus subtilis*. *FEMS Microbiol Rev* 2009; **33**: 152–63.

[22] Gray DA, Dugar G, Gamba P, Strahl H, Jonker MJ, Hamoen LW. Extreme slow growth as alternative strategy to survive deep starvation in bacteria. *Nat Commun* 2019; **10**: 1–12.

[23] Riva S, Polsinelli M, Falaschi A. A New Phage of *Bacillus subtilis* with Infectious DNA having Separable Strands. *J Mol Biol* 1968; **35**: 347–56.

[24] Baptista C, Santos MA, São-José C. Phage SPP1 reversible adsorption to *Bacillus subtilis* cell wall teichoic acids accelerates virus recognition of membrane receptor YueB. *J Bacteriol* 2008; **190**: 4989–96.

[25] São-José C, Lhuillier S, Lurz R, Melki R, Lepault J, Santos MA, et al. The ectodomain of the viral receptor YueB forms a fiber that triggers ejection of bacteriophage SPP1 DNA. *J Biol Chem* 2006; **281**: 11464–70.

[26] São-José C, de Frutos M, Raspaud E, Santos MA, Tavares P. Pressure Built by DNA Packing Inside Virions: Enough to Drive DNA Ejection in Vitro, Largely Insufficient for Delivery into the Bacterial Cytoplasm. *J Mol Biol* 2007; **374**: 346–55.

[27] Jakutyte L, Lurz R, Baptista C, Carballido-Lopez R, São-José C, Tavares P, et al. First steps of bacteriophage SPP1 entry into *Bacillus subtilis*. *Virology* 2012; **422**: 425–34.

[28] Fernandes S, Labarde A, Baptista C, Jakutytè L, Tavares P, São-José C. A non-invasive method for studying viral DNA delivery to bacteria reveals key requirements for phage SPP1 DNA entry in *Bacillus subtilis* cells. *Virology* 2016; **495**: 79–91.

bioRxiv preprint doi: https://doi.org/10.1101/2022.10.26.513911; this version posted October 26, 2022. The copyright holder for this preprint (which was not certified by peer review) is the author/funder, who has granted bioRxiv a license to display the preprint in perpetuity. It is made available under aCC-BY-NC-ND 4.0 International license.

[29] Montenegro MA, Trautner TA. In vivo transcription of *Bacillus subtilis* bacteriophage SPP1. *MGG Mol Gen Genet* 1981; **181**: 512–7.

[30] Pedré X, Weise F, Chai S, Lüder G, Alonso JC. Analysis of Cis and Trans acting elements required for the initiation of DNA replication in the *Bacillus subtilis* bacteriophage SPP1. *J Mol Biol* 1994; **236**: 1324–40.

[31] Chai S, Szepan U, Lüder G, Trautner TA, Alonso JC. Sequence analysis of the left end of the *Bacillus subtilis* bacteriophage SPP1 genome. *Gene* 1993; **129**: 41–9.

[32] Vinga I, Dröge A, Stiege AC, Lurz R, Santos MA. The minor capsid protein gp7 of bacteriophage SPP1 is required for efficient infection of *Bacillus subtilis*. *Mol Microbiol* 2006; **61**: 1609–21.

[33] Cvirkaite-Krupovic V, Carballido-López R, Tavares P. Virus Evolution toward Limited Dependence on Nonessential Functions of the Host: the Case of Bacteriophage SPP1. *J Virol* 2015; **89**: 2875–83.

[34] Zeigler DR, Rodriguez S, Chevreux B, Muffler A, Albert T, Bai R, et al. The origins of 168, W23, and other *Bacillus subtilis* Legacy Strains. *J Bacteriol* 2008; **190**: 6983–95.

[35] Yasbin RE, Fields PI, Andersen BJ. Properties of *Bacillus subtilis* 168 derivatives freed of their natural prophages. *Gene* 1980; **12**: 155–9.

[36] Schindelin J, Arganda-Carreras I, Frise E, Kaynig V, Longair M, Pietzsch T, et al. Fiji: An open-source platform for biological-image analysis. *Nat Methods* 2012; **9**: 676–82.

[37] Ducret A, Quardokus EM, Brun Y V. MicrobeJ, a tool for high throughput bacterial cell detection and quantitative analysis. *Nat Microbiol* 2016; **1**: 1–7.

[38] Labarde A, Jakutyte L, Blllaudeau C, Fauler B, Lopez-Sans M, Ponien P, et al. Temporal Compartmentalization of Viral Infection in Bacterial Cells. *Proc Natl Acad Sci* 2021; **118**: e2018297118.

[39] Droge A, Santos MA, Stiege AC, Alonso JC, Lurz R, Trautner TA, et al. Shape and DNA Packaging Activity of Bacteriophage SPP1 Procapsid: Protein Components and Interactions during Assembly. *J Mol Biol* 2000; **296**: 117–32.

[40] R Core Team. R: A Language and Environment for Statistical Computing. *R Found Stat Comput* 2020; **1**: 409.

[41] Muggeo VMR. Segmented: An R Package to Fit Regression Models with Broken-Line Relationships. *R News* 2008; **3**: 343–4.

[42] Hothorn T, Bretz F, Westfall P. Simultaneous inference in general parametric models. *Biometrical J* 2008; **50**: 346–63.

bioRxiv preprint doi: https://doi.org/10.1101/2022.10.26.513911; this version posted October 26, 2022. The copyright holder for this preprint (which was not certified by peer review) is the author/funder, who has granted bioRxiv a license to display the preprint in perpetuity. It is made available under aCC-BY-NC-ND 4.0 International license.

548 [43] Russell, L. (2019). emmeans: estimated Marginal Means, aka Least-Squares
549 Means. *R package version 1.4*. **3.01**.

550 [44] Weart RB, Lee AH, Chien AC, Haeusser DP, Hill NS, Levin PA. A Metabolic Sensor
551 Governing Cell Size in Bacteria. *Cell* 2007; **130**: 335–47.

552 [45] Chien AC, Zareh SKG, Wang YM, Levin PA. Changes in the oligomerization
553 potential of the division inhibitor UgtP co-ordinate *Bacillus subtilis* cell size with
554 nutrient availability. *Mol Microbiol* 2012; **86**: 594–610.

555 [46] Juillot D, Billaudeau C, Evouna-mengue P, Brodin P, Chastanet A. A high content
556 microscopy screening identifies genes involved in cell width control in *Bacillus*
557 *subtilis*. *mSystems* 2021; **6**: e01017-21.

558 [47] Strauch MA, Hoch JA. Signal transduction in *Bacillus subtilis* sporulation. *Curr Opin*
559 *Genet Dev* 1993; **3**: 203–12.

560 [48] São-José C, Baptista C, Santos MA. *Bacillus subtilis* operon encoding a membrane
561 receptor for bacteriophage SPP1. *J Bacteriol* 2004; **186**: 8337–46.

562 [49] Adams MH. Bacteriophages. Interscience Publishers, New York; 1959.

563 [50] Valero-Rello A, López-Sanz M, Quevedo-Olmos A, Sorokin A, Ayora S. Molecular
564 mechanisms that contribute to horizontal transfer of plasmids by the bacteriophage
565 SPP1. *Front Microbiol* 2017; **8**: 1–13.

566 [51] Alonso JC, Lüder G, Stiege AC, Chai S, Weise F, Trautner TA. The complete
567 nucleotide sequence and functional organization of *Bacillus subtilis* bacteriophage
568 SPP1. *Gene* 1997; **204**: 201–12.

569 [52] Godinho LM, El Sadek Fadel M, Monniot C, Jakutyte L, Auzat I, Labarde A, et al.
570 The Revisited Genome of *Bacillus subtilis* Bacteriophage SPP1. *Viruses* 2018; **10**:
571 705.

572 [53] Ignatiou A, Brasilès S, El Sadek Fadel M, Bürger J, Mielke T, Topf M, et al. Structural
573 transitions during the scaffolding-driven assembly of a viral capsid. *Nat Commun*
574 2019; **10**.

575 [54] Singh KD, Schmalisch MH, Stülke J, Görke B. Carbon catabolite repression in
576 *Bacillus subtilis*: quantitative analysis of repression exerted by different carbon
577 sources. *J Bacteriol* 2008; **190**: 7275–84.

578 [55] Abedon ST. Lysis from without. *Bacteriophage* 2011; **1**: 46–9.

579 [56] Fernandes S, São-José C. More than a hole: the holin lethal function may be
580 required to fully sensitize bacteria to the lytic action of canonical endolysins. *Mol*
581 *Microbiol* 2016; **102**: 92–106.

bioRxiv preprint doi: https://doi.org/10.1101/2022.10.26.513911; this version posted October 26, 2022. The copyright holder for this preprint (which was not certified by peer review) is the author/funder, who has granted bioRxiv a license to display the preprint in perpetuity. It is made available under aCC-BY-NC-ND 4.0 International license.

[57] Mahmoudabadi G, Milo R, Phillips R. Energetic cost of building a virus. *Proc Natl Acad Sci* 2017; **114**: e4324–33.

[58] Fernandes S, São-José C. Probing the function of the two holin-like proteins of bacteriophage SPP1. *Virology* 2017; **500**: 184–9.

[59] Yin J. A quantifiable phenotype of viral propagation. *Biochem Biophys Res Commun* 1991; **174**: 1009–14.

[60] Sillankorva S, Oliveira R, Vieira MJ, Sutherland I, Azeredo J. *Pseudomonas fluorescens* infection by bacteriophage phiS1: the influence of temperature, host growth phase and media. *FEMS Microbiol Lett* 2004; **241**: 13–20.

[61] Melo LDR, França A, Brandão A, Sillankorva S, Cerca N, Azeredo J. Assessment of *Sep1virus* interaction with stationary cultures by transcriptional and flow cytometry studies. *FEMS Microbiol Ecol* 2018; **94**: 1–8.

[62] Koskella B, Hernandez CA, Wheatley RM. Understanding the Impacts of Bacteriophage Viruses: From Laboratory Evolution to Natural Ecosystems. *Annu Rev Virol* 2022; **9**: 1–22.

[63] Ripp S, Miller R V. The role of pseudolysogeny in bacteriophage-host interactions in a natural freshwater environment. *Microbiology* 1997; **143**: 2065–70.

[64] Williamson KE, Fuhrmann JJ, Wommack KE, Radosevich M. Viruses in Soil Ecosystems: An Unknown Quantity Within an Unexplored Territory. *Annu Rev Virol* 2017; **4**: 201–19.

[65] Chevallereau A, Pons BJ, van Houte S, Westra ER. Interactions between bacterial and phage communities in natural environments. *Nat Rev Microbiol* 2022; **20,** 49–62

bioRxiv preprint doi: https://doi.org/10.1101/2022.10.26.513911; this version posted October 26, 2022. The copyright holder for this preprint (which was not certified by peer review) is the author/funder, who has granted bioRxiv a license to display the preprint in perpetuity. It is made available under aCC-BY-NC-ND 4.0 International license.

Figure Legends

Fig. 1 SPP1 infection of *B. subtilis* during exponential, transition and stationary phase. a Infection experiment setup. White bars represent growth of uninfected cultures up until infection (orange phage symbols, time-point adjacent) during the bacterial growth phase indicated on the left, as defined in **Supplementary figure 2**. Following infection, both one non-infected culture and one infected culture were then followed for the duration shown on the right of each arrow. The timing of each infection during the growth of *B, subtilis* is marked on the growth curve displayed to the right of the panel. **b** OD_{600} curves of Bs^{wt} grown in flasks in LB medium at 37°C and infected with an input of 2×10^9 pfu ml^{-1} of $SPP1^{wt}$ (orange triangles) at the time-points indicated in **a**. Infection was monitored for 2 h. Control growth curves of non-infected bacteria are in grey. **c** Titre of free phage PFU at the end of each infection in **b.** The dashed line indicates the input of PFU used for infection. **d** OD_{600} curve of Bs^{wt} infected in SP for 18h as represented schematically in **a**. **e** Titre of free phage PFU after 2 and 18h p.i. in SP. Data in **b**-**e** are from three independent biological replicates. Linear regression models fit to the data for statistical analysis in **b** and **d** are represented graphically by dotted lines (model fit) and shaded areas (95% confidence intervals). The mean (horizontal lines) and standard deviation (vertical bars) are displayed in **b** and **d**. The median, upper and lower quartiles (boxes) and the limits of the data (whiskers) of the data are given in **c** and **e**. Additional data and analyses related to these experiments are provided in **Table S3** and **Supplementary Data Analysis**. Colour version of figure available online.

Fig. 2 Long-term observation of growth and lysis of *B. subtilis* infected during exponential, transition and stationary phase. a OD_{600} curves of Bs^{wt} cultures grown in a 96-well plate and monitored continuously in a plate reader. Bacteria were infected with 2×10^9 pfu ml^{-1} of $SPP1^{wt}$ at different phases of the *B. subtilis* growth cycle (orange triangles). Infection times differ slightly from experiments performed in flasks (see **Fig. 1**) to take into account the lower growth rate of cultures in 96-well plates. Sharp peaks in OD_{600} are due to settling of cells when plates were removed for infection with SPP1. Control growth curves of non-infected bacteria are in grey. An example of the times taken to reach 50% of the maximum OD_{600} (50% lysis) and for lysis to stop (100% lysis) in EP infection is displayed (see **Supplementary Material and Methods**). **b** Lysis behavior features extracted from the

bioRxiv preprint doi: https://doi.org/10.1101/2022.10.26.513911; this version posted October 26, 2022. The copyright holder for this preprint (which was not certified by peer review) is the author/funder, who has granted bioRxiv a license to display the preprint in perpetuity. It is made available under aCC-BY-NC-ND 4.0 International license.

data in **a**. Tukey's honest significant difference contrasts (THC's) are displayed to the left of the table and are identical for both data columns. Statistical significance levels; *** $p < 0.001$. Non-significant differences are not shown. Data are from three independent biological replicates. Means (dotted line in **a**) and standard deviations (shaded areas in **a**) are displayed in both panels. Data and analyses related to these experiments are presented in **Table S3** and **Supplementary Data Analysis**. Colour version of figure available online.

Fig. 3 SPP1 infection dynamics during prolonged stationary phase infection of *B. subtilis*. *Bs*^{wt} bacteria grown in flasks with LB medium at 37°C were infected with 2×10^9 pfu ml^{-1} of SPP1^{mNeonGreen} at 10h post-inoculation (green phage symbol in **a**). Bacterial density (OD_{600} in **a** and CFU ml^{-1} in **b**), total and free phage (PFU ml^{-1}) (**c**), and the number of visibly infected bacteria (**d**, **e**) were monitored until 30h p.i., in parallel. The number and percentage of CFU originating from spores was also quantified (grey squares for non-infected culture and green diamonds for infected culture in **b**; ordinate on the right). Individual infected cells were counted at each time-point by microscopy (orange arrowheads in **d**, identifying bright cells in the mNeonGreen channel) and the percentage of infected cells in the infected culture determined (**e**). The white scale bars represent 10µm. Sample sizes were as follows; 0h; n = 510, 1h; n = 630, 2h; n = 816, 4h; n = 658, 6h; n = 967, 8h; n= 780, 10h; n = 764, 30h; n = 241. Data are from three independent biological replicates. Linear regression models fit to the data for statistical analysis in **a**, **c** and **e** are represented graphically by dotted lines (model fit) and shaded areas (95% confidence intervals). The mean (horizontal lines) and standard deviation (vertical bars) are displayed in **a**, **c** and **e**. The median, upper and lower quartiles (boxes) and the limits of the data (whiskers) of the data are given in **b**. Data and analyses related to these experiments are detailed in **Table S3** and **Supplementary Data Analysis**. Colour version of figure available online.

Fig. 4 The impact of irreversible adsorption efficiency on stationary phase infection dynamics. a Irreversible adsorption (IA) of SPP1^{wt} at different phases of *Bs*^{wt} (grey circles) and *Bs*$^{Pspac::yueB}$ (magenta diamonds) growth. IA was quantified as described [24] using bacterial growth medium (dark grey squares) as control for residual phage particle loss during manipulation. THC's are displayed above the plot. Sampling points during bacterial growth are presented in **Supplementary figure 5a**. **b** Growth and lysis of bacteria infected

bioRxiv preprint doi: https://doi.org/10.1101/2022.10.26.513911; this version posted October 26, 2022. The copyright holder for this preprint (which was not certified by peer review) is the author/funder, who has granted bioRxiv a license to display the preprint in perpetuity. It is made available under aCC-BY-NC-ND 4.0 International license.

673 with 2×10^9 PFU ml^{-1} SPP1^{wt} (orange phage symbol) during SP in a 96-well plate monitored
674 by OD_{600} measurements in a plate reader. Data points of non-infected or infected *Bs*^{wt} and
675 *Bs*$^{Pspac::yueB}$ are represented by the symbols shown in the inset. **c** Growth and lysis of
676 bacteria infected during SP with 2×10^9 PFU ml^{-1} SPP1^{mNeonGreen} (green phage symbol, for
677 comparison with SPP1^{mNeonGreen} infections in **Fig. 3a**) in flasks was monitored by OD_{600}
678 measurement. Symbols are as in **b**. Vertical arrows identify sampling time points for free
679 and total PFU titration. **d**,**e** Titration of free and total infectious SPP1 particles, respectively,
680 sampled at the time points shown in **c**. The dashed green line shows the input phages added
681 for infection. Data in all panels are from three independent biological replicates. The median,
682 upper and lower quartiles (boxes) and the limits of the data (whiskers) of the data are given
683 in panel **a**. The mean (dotted lines) and standard deviation (shaded areas) are displayed in
684 panel **b**. The mean (horizontal lines) and standard deviation (vertical bars) are displayed in
685 panels **c**-**e**. Piece-wise linear regression models were fit to OD_{600} and PFU data for analysis
686 (dotted lines (model fits) and shaded areas (confidence intervals) in **c**-**e**). Data and statistical
687 analyses related to these experiments are provided in **Table S3** and **Supplementary Data**
688 **Analysis**.
689

690 **Fig. 5 SPP1 gene expression during exponential and stationary phase infection. a**
691 Bacteriophage SPP1 genetic map. Early (light blue) and late genes (salmon) investigated in
692 this study are highlighted. Functional classes of genes involved in different steps of SPP1
693 infection are identified by coloured bars annotated in the legend on the right. Early promoters
694 (*P*E1 to *P*E5; blue) and the late promoters *P*L1/*P*L2 (salmon) are labeled below. Note that
695 *P*L1/*P*L2 control the transcription of the late DNA packaging genes and gene *6* displayed on
696 the left in the linear representation of the SPP1 genome. **b** Quantification of phage gene
697 expression by qRT-PCR from *Bs*^{wt} during EP and SP phases infected with SPP1^{mNeonGreen}
698 (**Supplementary figure 6a,d**). Samples of EP cultures were taken at 8 and 25min post-
699 infection while SP cultures were sampled at 1, 6, 10 and 30h p.i.. Data were calibrated
700 ('calibrator') to the gene expression of non-infected EP bacteria (*top*) and to that of infected
701 EP bacteria at 8 min p.i. (*bottom*). The expression of early genes *35* and *46* (blue symbols),
702 and of late genes *6*, *11*, *24.1* and *26* (magenta symbols) was quantified as described in detail
703 in **Supplementary Materials and Methods**. THC's are displayed above the plots.
704 Statistical significance levels: * $p < 0.05$, ** $p < 0.01$, *** $p < 0.001$. **c** Production of procapsid

bioRxiv preprint doi: https://doi.org/10.1101/2022.10.26.513911; this version posted October 26, 2022. The copyright holder for this preprint (which was not certified by peer review) is the author/funder, who has granted bioRxiv a license to display the preprint in perpetuity. It is made available under aCC-BY-NC-ND 4.0 International license.

scaffolding protein gp11 in EP and SP-infected bacteria. Samples were taken from the same cultures and time-points as RNA used for qRT-PCR in **b**. Total protein was stained with Coomassie blue in SDS-PAGE gels (left) and gp11 was detected specifically in western blots with anti-gp11 antibodies (right). Gel loading was normalised using an identical amount of total protein. Data in **b** are from three independent biological replicates. Data in **c** are representative of three independent Coomassie-stained gels and Western blots. The mean (horizontal lines) and standard deviation (vertical bars) are displayed in **b**. Data and analyses related to these experiments are detailed in **Table S3** and **Supplementary Data Analysis**. Colour version of figure available online.

Fig. 6 Influence of nutrient supplementation on stationary phase infection of *B. subtilis* by SPP1. a Experimental setup used to assess the effect of adding the carbon source maltose to SP bacteria non-infected (grey) and infected with SPP1 (orange). Phage infection is denoted by the orange phage symbol and times of maltose addition by the letter 'M'. **b** OD_{600nm} curves of Bs^{wt} cultures grown in a 96-well plate and monitored continuously in a plate reader. Bacteria were infected with 2×10^9 pfu ml^{-1} of $SPP1^{wt}$ at 11h post-inoculation (SP) (orange triangles) and supplemented, in some cases, with 15mM maltose (triangles are coloured in variations of orange as the vertical arrows in **a**, dependent on the time of addition of maltose). Growth curves of non-infected bacteria supplemented with maltose (variations of dark grey according to the vertical arrows greyscale in **a**) or not supplemented (light grey) are also displayed. The orange phage symbol denotes the time of infection, blue arrows denote times of maltose addition and the black arrow the time of titration of PFU. **c** Titre of total (circles) and free phages (triangles) at 29h p.i. from the experiments in **b**. Color code is as in **a** and **b**. A dashed line displays the phage input for infection. **d** Titre of total and free phages at 30h p.i. of Bs^{wt} grown and infected at SP in flasks as in **Fig. 3**. The infection and maltose addition time-points were adapted to flask infection conditions. Data display is as in **c**. Data are from three independent biological replicates. The mean (dotted lines) and standard deviation (shaded areas) are displayed in panel **b**. The median, upper and lower quartiles (boxes) and the limits of the data (whiskers) of the data are given in panels **c,d**. Data and analyses related to these experiments are detailed in **Table S3** and **Supplementary Data Analysis**. Colour version of figure available online.

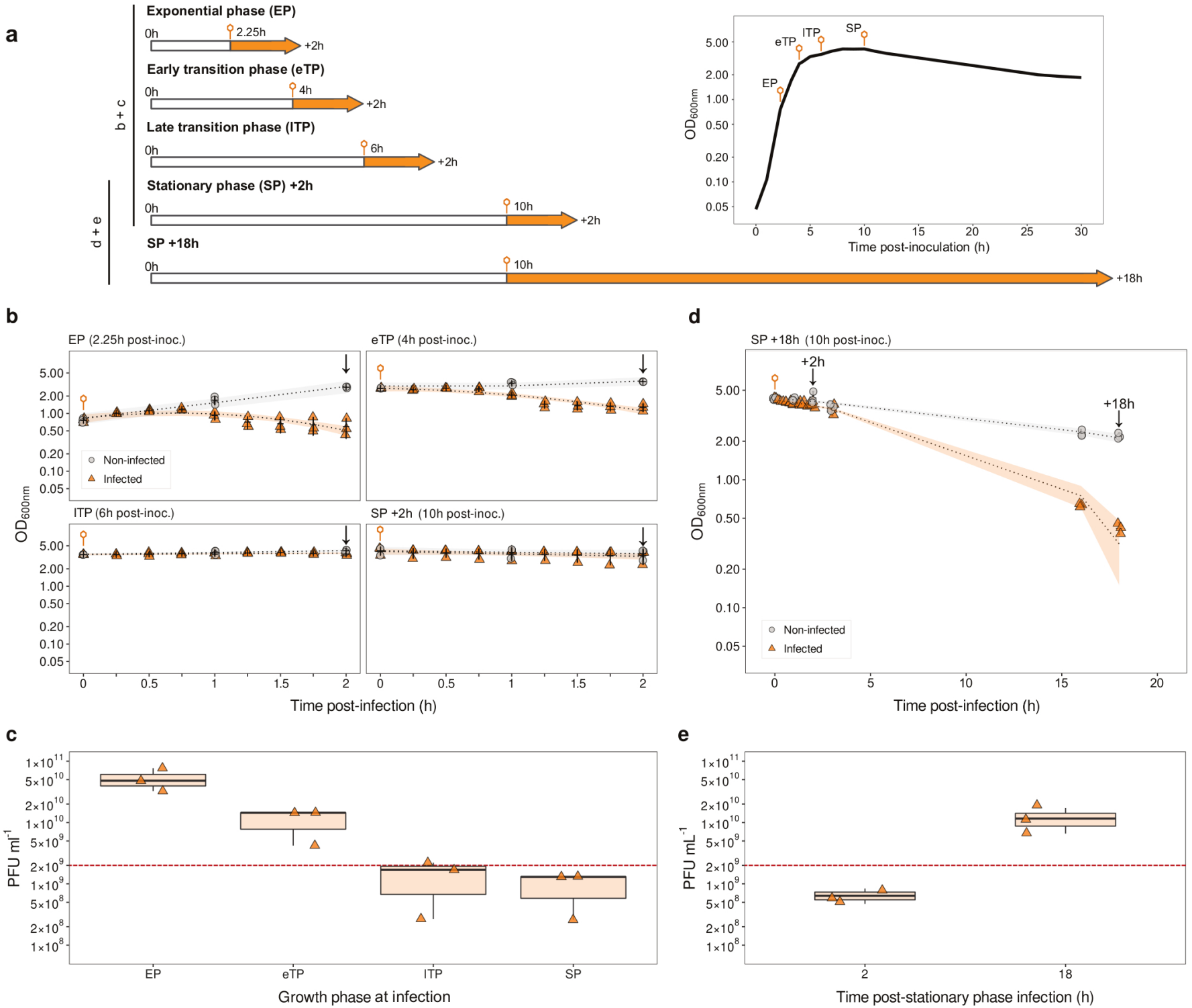
a
Exponential phase (EP)
0h
2.25h
+2h
Early transition phase (eTP)
0h
4h
+2h
Late transition phase (ITP)
0h
6h
+2h
b + c
Stationary phase (SP) +2h
0h
10h
+2h
d + e
SP +18h
0h
10h
+18h
EP
eTP
ITP
SP
OD600nm
Time post-inoculation (h)
b
EP (2.25h post-inoc.)
eTP (4h post-inoc.)
ITP (6h post-inoc.)
SP +2h (10h post-inoc.)
Non-infected
Infected
OD600nm
Time post-infection (h)
d
SP +18h (10h post-inoc.)
+2h
+18h
Non-infected
Infected
OD600nm
Time post-infection (h)
c
PFU ml-1
EP
eTP
ITP
SP
Growth phase at infection
e
PFU mL-1
2
18
Time post-stationary phase infection (h)

Figure 1

bioRxiv preprint doi: https://doi.org/10.1101/2022.10.26.513911; this version posted October 26, 2022. The copyright holder for this preprint (which was not certified by peer review) is the author/funder, who has granted bioRxiv a license to display the preprint in perpetuity. It is made available under aCC-BY-NC-ND 4.0 International license.

a

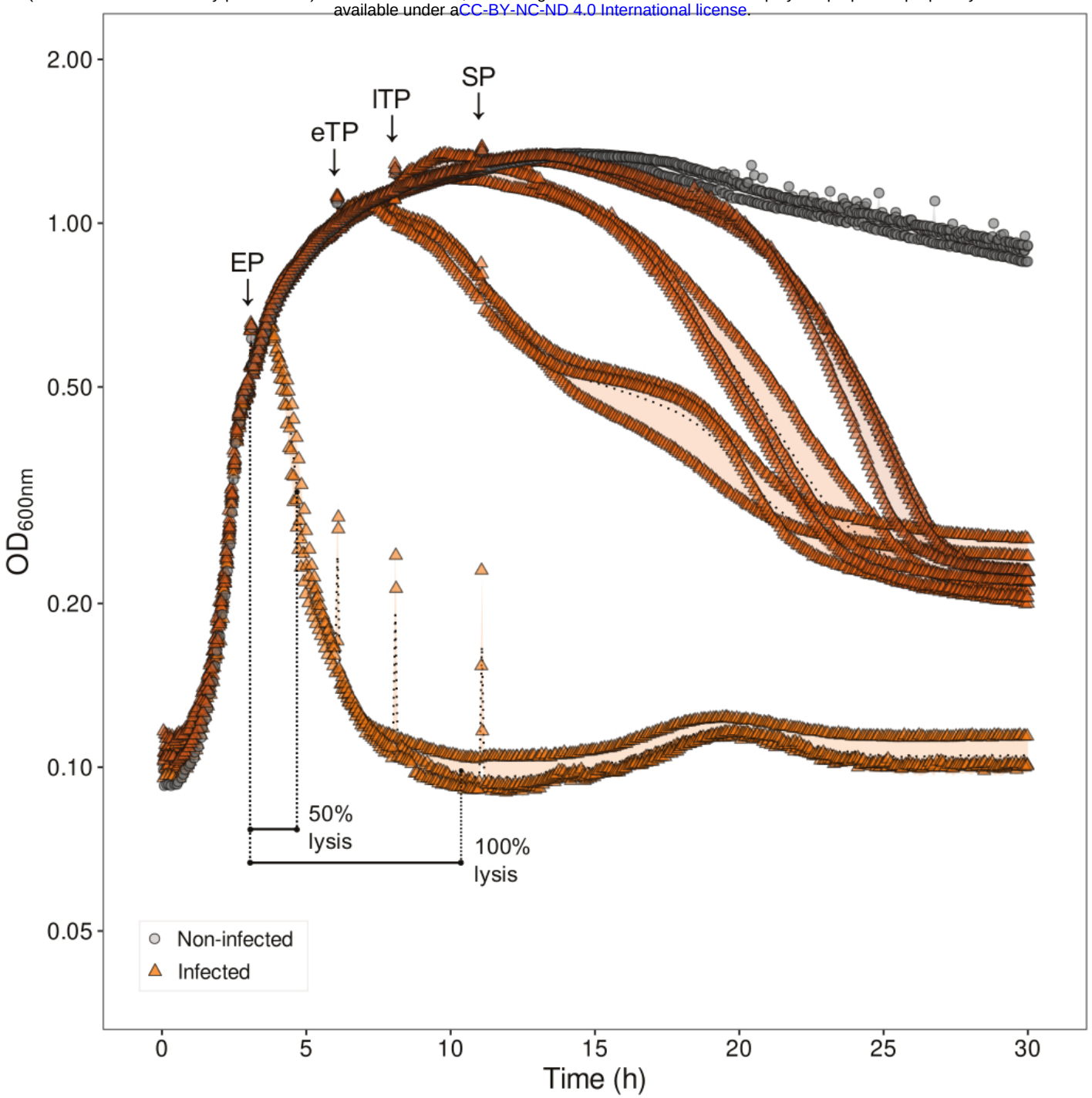

b

Growth phase	Infection time (h)	50% lysis[1] (h)	100% lysis[2] (h)	Lysis behaviour
EP	3	1.72 ± 0.173	7.31 ± 0.898	monophasic
eTP	4	7.67 ± 0.583	18.1 ± 1.67	multiphasic (slow → fast)
ITP	6	10.8 ± 0.962	18.4 ± 1.06	biphasic (slow → fast)
SP	10	11.7 ± 0.417	17.3 ± 0.763	biphasic (slow → fast)

***
***
***
***

Figure 2

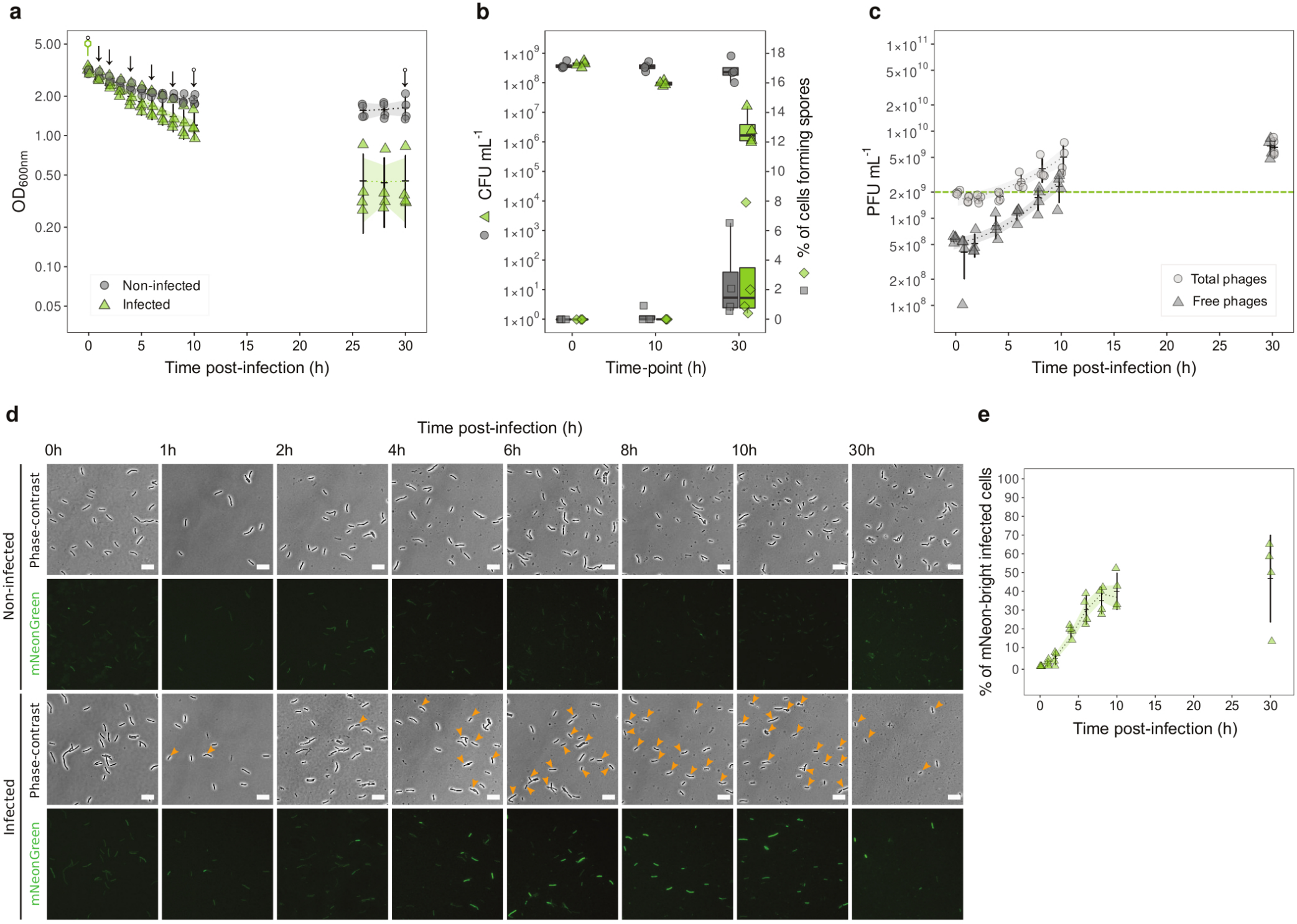
a
b
c
d
e
OD600nm
Time post-infection (h)
Non-infected
Infected
CFU mL-1
% of cells forming spores
Time-point (h)
PFU mL-1
Total phages
Free phages
Time post-infection (h)
0h
1h
2h
4h
6h
8h
10h
30h
Non-infected
Infected
Phase-contrast
mNeonGreen
% of mNeon-bright infected cells
Time post-infection (h)

Figure 3

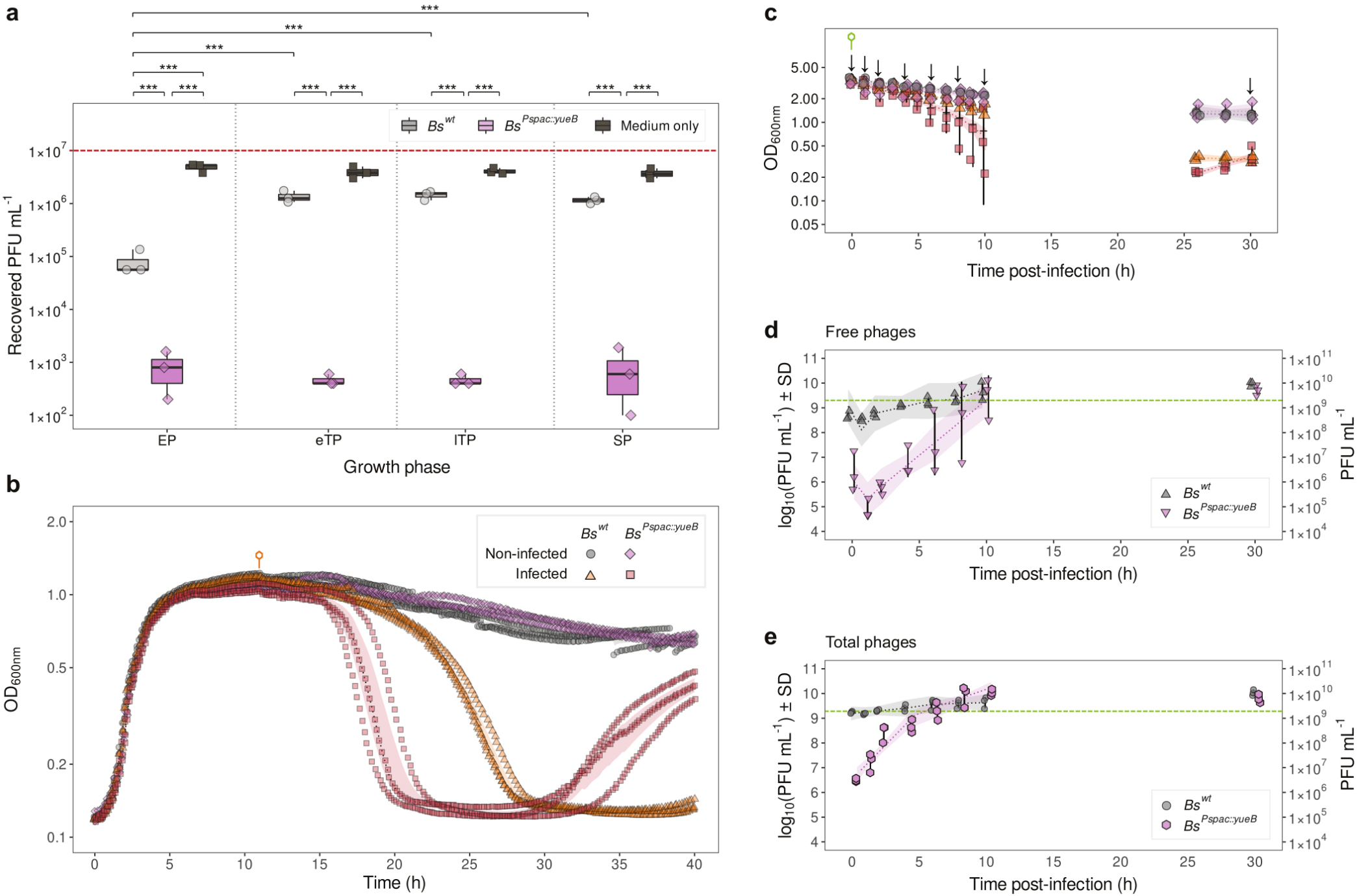
a
***
***
***
***
***
***
***
***
***
***
***
Bs^wt
Bs^Pspac::yueB
Medium only
Recovered PFU mL^-1
1×10^7
1×10^6
1×10^5
1×10^4
1×10^3
1×10^2
EP
eTP
ITP
SP
Growth phase
b
Bs^wt
Bs^Pspac::yueB
Non-infected
Infected
OD600nm
2.0
1.0
0.5
0.2
0.1
0
5
10
15
20
25
30
35
40
Time (h)
c
OD600nm
5.00
2.00
1.00
0.50
0.20
0.10
0.05
0
5
10
15
20
25
30
Time post-infection (h)
d
Free phages
log10(PFU mL^-1) ± SD
PFU mL^-1
Bs^wt
Bs^Pspac::yueB
Time post-infection (h)
e
Total phages
log10(PFU mL^-1) ± SD
PFU mL^-1
Bs^wt
Bs^Pspac::yueB
Time post-infection (h)

Figure 4

bioRxiv preprint doi: https://doi.org/10.1101/2022.10.26.513911; this version posted October 26, 2022. The copyright holder for this preprint (which was not certified by peer review) is the author/funder, who has granted bioRxiv a license to display the preprint in perpetuity. It is made available under aCC-BY-NC-ND 4.0 International license.

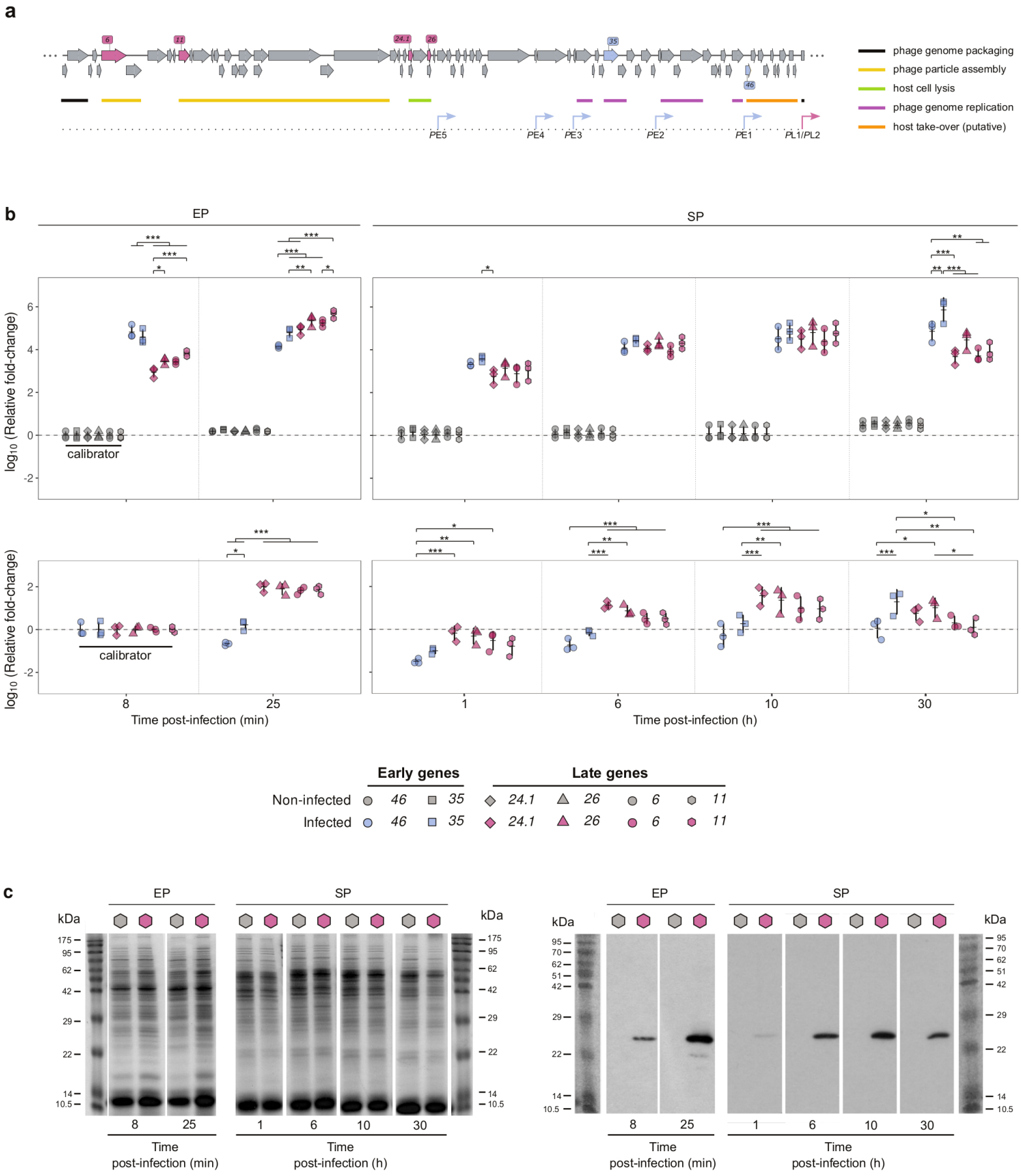

Figure 5

bioRxiv preprint doi: https://doi.org/10.1101/2022.10.26.513911; this version posted October 26, 2022. The copyright holder for this preprint (which was not certified by peer review) is the author/funder, who has granted bioRxiv a license to display the preprint in perpetuity. It is made available under aCC-BY-NC-ND 4.0 International license.

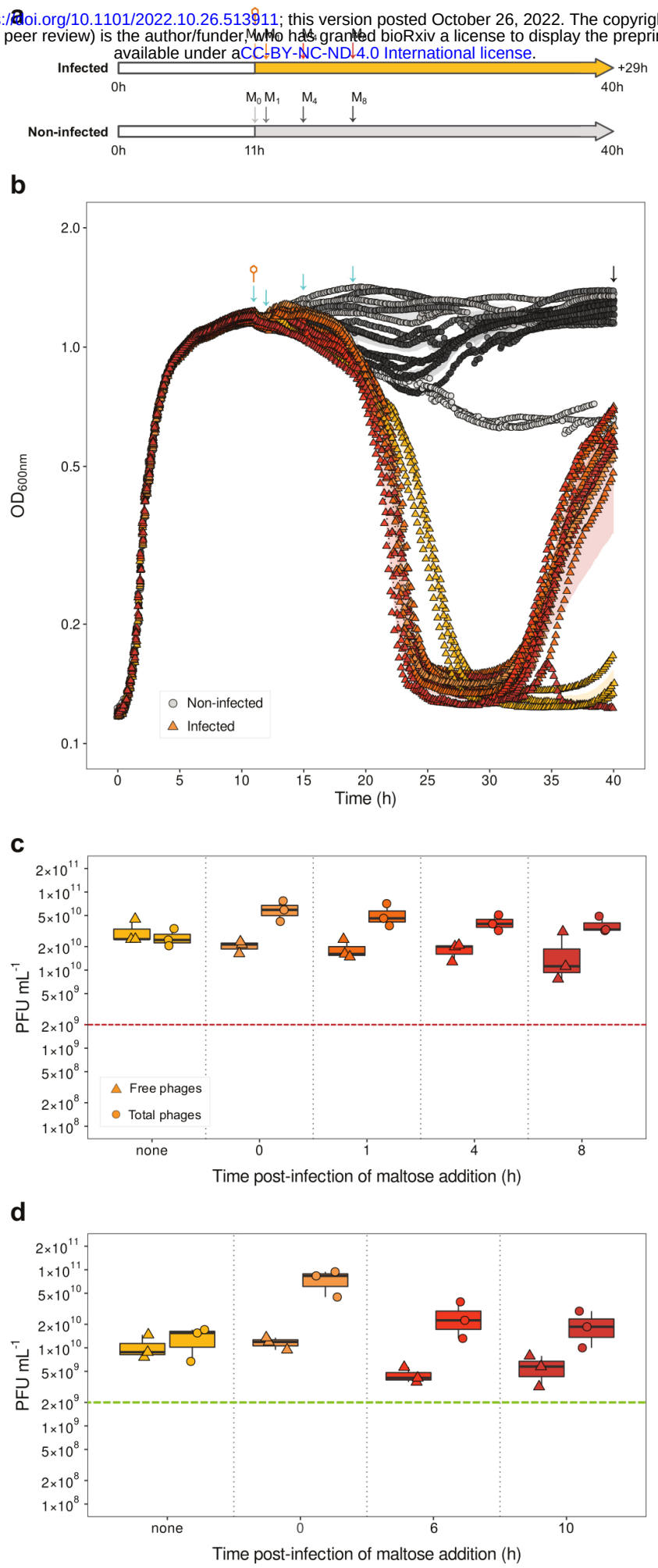

Figure 6